MOLECULAR, GENETIC, AND BIOCHEMICAL ANALYSIS OF THE PHIKT DISRUPTIN: A NEW CLASS OF LYSIS PROTEINS

An Undergraduate Research Scholars Thesis

by

CODY MARTIN

Submitted to the Undergraduate Research Scholars program at
Texas A&M University
in partial fulfillment of the requirements for the designation as an

UNDERGRADUATE RESEARCH SCHOLAR

Approved by Research Advisor: Dr. Ry Young

May 2019

Major: Biochemistry
Genetics

TABLE OF CONTENTS

Page

ABSTRACT

Molecular, Genetic, and Biochemical Analysis of the PhiKT Disruptin: A New Class of Lysis Proteins

Cody Martin
Department of Biochemistry and Biophysics
Texas A&M University

Research Advisor: Dr. Ry Young
Department of Biochemistry and Biophysics
Texas A&M University

Phages are the viruses of bacteria. To complete the infection cycle, phages produce lysis proteins to overcome the bacterial cell envelope. The final barrier in Gram-negative hosts is the outer membrane (OM). We have recently identified a novel lysis protein produced by the phage PhiKT called gp28. Our previous results indicate that gp28 is produced to disrupt the outer membrane (OM). Based on similarities with cathelicidin antimicrobial peptides (CAMPs) like LL-37, such as helical content, cationic charge, membrane association, and short peptide length (<60 aa), our model is that gp*28* is a phage-encoded AMP. We hypothesized that, like other CAMPs, gp*28* disrupts both the IM and OM. We developed a kinetic assay using fluorescence microscopy to report membrane permeabilization. The results indicate that gp*28* permeabilizes the IM before the OM. To further investigate how gp*28* disrupts membranes, we conducted a mutational study of gene *28*, using complementation of a spanin defect as an assay. Our results indicate that disruption of structures characteristic of CAMPs resulted in loss of function. Future work will probe subcellular localization of mutants using fluorescence microscopy to investigate determinants of membrane interaction.

ACKNOWLEDGEMENTS

I would like to thank my advisor, Dr. Ry Young, and my two mentors, Drs. Jolene Ramsey and Jesse Cahill, for their support throughout my research endeavors.

I would also like to thank the entirety of the Center for Phage Technology lab members, as well as friends and family.

Finally, thanks to the Arnold and Mabel Beckman Foundation for providing an academic scholarship and research funding to foster my undergraduate research career.

NOMENCLATURE

IM	Inner membrane
PG	Peptidoglycan
OM	Outer membrane
AMP	Antimicrobial peptide
S	λ Holin gene
R	λ Endolysin gene
Rz	λ Inner spanin gene
Rz1	λ Outer spanin gene
OD	Optical density
LB	Luria-Bertani
ThT	Thioflavin-T
FlAsH-EDT_2	Fluorescein arsenical hairpin binding bis-EDT (ethanedithiol) adduct
TC	Tetracysteine

FIGURES

FIGURES Page

TABLES

TABLES Page

CHAPTER I

INTRODUCTION

Bacteriophages and λ lysis

Phages are the viruses of bacteria. The life cycle of a phage involves infecting a host, replicating using the host cellular machinery, and bursting out of the bacteria in an explosive event known as lysis. Lysis is the last step in the phage life cycle in which newly produced phages overcome the host-cell barriers to release progeny. The three barriers of the Gram-negative bacterial cell envelope that must be overcome by phages are the inner membrane (IM), peptidoglycan (PG), and outer membrane (OM). Phage λ is a temperate double-stranded DNA phage that infects *Escherichia coli.* Much of the knowledge about lysis is the result of studies done with this paradigm phage and host. One reason for this is the ease of genetic manipulations of both λ and *E. coli*. The temperate-sensitive λ allele cI_{857} represses transcription of the late genes at temperatures below 36ºC (1). Repression of the late genes allows λ to potentially enter the lysogenic cycle (2), characterized by integration of the phage genome within the bacterial chromosome for dormancy. Above 36ºC, the cI_{857} repressor is inactivated, causing expression of the late genes that will activate the virulent cycle, ultimately leading to lysis (2). For biological processes under temporal regulation such as phage assembly, genes are classified as early, middle, or late. As might be expected, phage lysis genes are late genes to ensure that phage morphogenesis occurs before the host is destroyed. To achieve lysis, phage λ produces four proteins (3). The first λ lysis protein encoded by *S* is the holin. Holins control the timing of lysis by opening a hole in the first barrier, the IM. Before lysis, holins are dispersed throughout the IM. At a genetically programmed time, holins oligomerize primarily at a pole of the cell to form

a raft (4) that initiates the creation of a micron-scale hole. This hole allows the release of the second λ lysis protein encoded by *R* called the endolysin. The endolysin then degrades the PG (2). The endolysin is a cytoplasmic protein which cannot cross an intact IM. Thus, endolysin-mediated degradation of the PG is dependent on the holin hole. The final step is disruption of the OM by the final two λ lysis proteins encoded by *Rz and Rz1*, respectively. *Rz* encodes the i-spanin, and *Rz1* encodes the o-spanin. The Rz and Rz1 proteins form a heterotetramer that completes the process of lysis, resulting in a local blowout to release progeny virions (5). The events of wild-type (WT) λ lysis occur in quick succession such that no morphological changes are observed immediately prior to lysis.

Spanins

Spanins have distinct structures and topology

λ spanins are composed of two subunits: the i-spanin and o-spanin. *Rz* encodes the i-spanin, and *Rz1* encodes the o-spanin. The Rz protein is a class II IM protein with an N-terminal transmembrane domain (TMD) and a C-terminal periplasmic domain. The periplasmic domain of Rz contains 37% acidic and basic residues. Two stretches of α-helices, separated by a linker region, compose the Rz periplasmic domain. The Rz1 protein is a proline-rich OM lipoprotein with an N-terminal lipoylation signal sequence. Because of the large amount of proline residues, the Rz1 protein is expected to be unstructured (6). Unlike the two-component λ spanins, unimolecular spanins (u-spanins) are only composed of a single spanin protein. U-spanins have an N-terminal lipoylation sequence similar to Rz1. A distinguishing feature of u-spanins is the C-terminal TMD. Neither spanin subunit in the two-component system possess a C-terminal TMD. Additionally, u-spanins are predicted to consist of primarily β-sheets in the periplasmic domains (7). Mutational analysis of Rz and Rz1 reveal that the α-helices and proline-rich regions of Rz

and Rz1, respectively, are vital for spanin function (8). Before association with its cognate partner, Rz exists as a homodimer *in vivo*. Likewise, Rz1 is a homodimer before formation of the Rz-Rz1 complex. The dimerization of two Rz or Rz1 subunits is achieved by disulfide bonds from cysteine residues (9). Then, an Rz homodimer and Rz1 homodimer dimerize via their C-termini, forming a heterotetramer. The spanin heterotetramer spans the entire periplasm, hence the name.

Spanin function

Before the holin triggers, spanin complexes accumulate in the membranes, nested within the lacunae of the PG. Only when R degrades the PG can the complexes freely move laterally throughout the periplasm. Subsequent conformational changes in the spanin complex result in OM disruption and consequently lysis. Spanin function is, therefore, independent of S function. Studies with endolysins secreted to the periplasm independent of the S hole, such as signal anchor release (SAR) endolysins of phage 21, support the claim that spanins can act independently of holins (5). We later use the holin-independent function of the λ OM disruptors as an assay to probe for the presence of non-spanin OM disruptors in other phage (see section: Preliminary spanin-less phages) (10).

In contrast to WT λ lysis, *E. coli* lysogens with nonfunctional spanins exhibit a rod-to-sphere shape transition when lysis would normally occur. The shape change is because of the endolysin-mediated destruction of the PG. The OM is the only barrier of the cell envelope left, resulting in the entropically favored spherical shape. In addition to holin-independent function, we exploit the nonfunctional spanin phenotype as an assay to probe for OM disruption capacity in phages that do not possess spanins (see section: Preliminary spanin-less phages) (10).

The mechanism by which spanins achieve OM disruption has not directly been observed; however, there is evidence that spanins have fusogenic properties (11). As mentioned above, destruction of the PG by endolysin muralytic activity causes free movement that allows for coiled-coil oligomerization of spanin heterotetramers. Coiled-coil oligomerization is reported to bring membranes in closer proximity to facilitate fusion in eukaryotic systems (12,13). The fusogenic properties and α-helical coiled-coil domains of two-component spanins led to the model that they function similarly to class I viral fusion proteins (14,15) by fusing the IM and OM (8).

Spanins have genetic architectures useful for bioinformatic analysis

Nearly all phages that infect Gram-negative hosts must disrupt the OM to release progeny. Thus, these phages are expected to have an OM disruptor. However, recent bioinformatic analysis indicates 13% of phages do not have any detectable spanin genes (16). Our bioinformatic tool searches for sequence similarity to common structural motifs such as N-terminal TMDs for i-spanins, N-terminal lipoylation sequences for o-spanins and u-spanins, and C-terminal TMDs for u-spanins. Additionally, for two-component spanins, the unusual genetic architecture provides another genetic trail to follow. Like many other two-component spanins, the gene for Rz1 is nested within the +1 reading frame of Rz (6). The uncommon genetic architecture appears to reflect evolutionary pressure to conserve genomic space (17). Structural motifs are predicted from amino acid sequence. Phages that lack proteins with the above structural criteria, therefore, do not have detectable spanins. However, since lysis is an essential process of the infection cycle for all tailed phages (18), our hypothesis was that these spanin-less phages most likely have a unique OM disruptor. Thus, there could be an alternate mechanism for OM disruption. We then chose representative spanin-less phages for testing.

Preliminary spanin-less phages

Phage Petty possesses a putative non-spanin OM disruptor

To investigate the OM disruptors of a representative spanin-less phage, phage Petty was selected. The Petty lysis phenotype first was compared to the lysis phenotype of λ. Infections of *Acinetobacter* by Petty result in lytic blowouts that were monitored on a single-cell level to verify that the lysis phenotypes of Petty and the paradigm phage λ were essentially identical (19). Since Petty lysis does not stall at the OM disruption step as would infections with nonfunctional OM disruptors, Petty must have a non-spanin OM disruptor. *Acinetobacter*, however, is not a genetically facile system, so our strategy was to transition to a genetically tractable model system like *E. coli*.

Phage PhiKT possesses a putative non-spanin OM disruptor called gp28

We, therefore, selected PhiKT as a representative spanin-less phage that infects *E. coli* for testing (20). The PhiKT gp*28* protein has been shown in preliminary studies to support OM disruption of Gram-negative bacterial hosts, complementing the lysis defect of nonfunctional spanins in λ (10). From sequence analysis, gp*28* is a 56 amino acid protein this is highly cationic, with a net +7 charge at physiological pH (Figure 1A). From structural predictions, gp28 is expected to be helical, consisting of three helices connected by linker regions, predicted by JPred4 to be toward the N-terminus, middle, and C-terminus of gp28 (Figure 1A). The predicted helical sequences were then applied to the helical wheel prediction software HeliQuest. The helical pinwheel diagrams were generated suggest gp28 is amphipathic and membrane-associated. (Figure 1B-D).

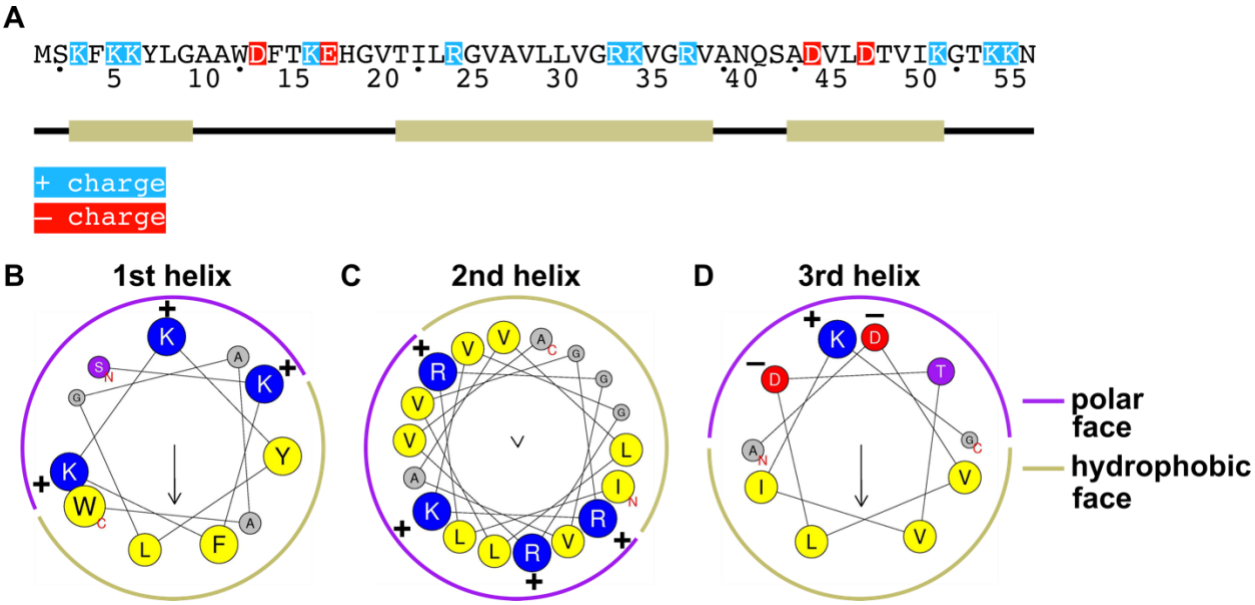

Figure 1. Gp28 is helical, cationic, and amphipathic. A) The amino acid sequence of gp28, highlighting charged residues atop α-helices predicted by JPred 4 (21). The helical wheel diagrams for the **B)** first, **C)** second, and **D)** third helices predicted by HeliQuest (22). These helical wheel diagrams depict predicted polar and hydrophobic faces. The helical residues are noted in **A)** by dots underneath the N- and C-terminal residue. The first helix shows residues S2–W12. The second helix shows residues I22–A39. The third helix shows residues A43–G52. The hydrophobic moment, μH, of each helix is 0.539, 0.017, and 0.563, respectively. Values close to 0 indicate amphipathic structure, while numbers above 0.3 indicate membrane association (23).

In fact, gp28 has been shown to associate with the membrane *in vivo* and *in vitro* by hydrophobic interactions as determined in cell fractionation assays using ultracentrifugation (10).

PhiKT gp28: phage-encoded AMP

Antimicrobial peptides

AMPs are molecules produced by innate immune system of multicellular organisms for defense against microorganisms (24). Cathelicidins are a class of AMPs commonly produced by mammals (25). Cathelicidins are produced as propeptides with a secretion signal sequence and a highly conserved cathelin N-terminal domain that inactivates the C-terminal antimicrobial domain (26). Cleavage of the signal sequence localizes cathelicidins to granules in an inactive

form. Removal of the cathelin domain produces the active C-terminal AMP (27). hCAP-18 is the only human cathelicidin (28). hCAP-18 is stored in granules of neutrophils, which are cells of the innate immune system. When neutrophils were induced to secrete granular material and activated by inflammatory chemicals that would be present during infection, hCAP-18 is cleaved by the serine protease proteinase 3 (27). Upon processing hCAP-18, the remaining 37 C-terminal residues become active, referred to as LL-37. LL-37 is the only cathelicidin AMP produced by humans (28). The bactericidal residues of cathelicidins have the following structural characteristics: <50 aa, cationic, amphipathic, and α-helical conformations upon membrane binding (29-31). The first binding sites of many cationic AMPs are lipopolysaccharides (LPS) in the outer leaflet of the OM of Gram-negative cells because bacterial LPS are negatively charged. Thus, AMPs are sensitive to changes in the composition of LPS (32). While the exact mechanisms of AMP membrane disruption are unknown, AMPs are known to be general membrane disruptors. Exogenous addition of LL-37 has been shown to first permeabilize the OM before the IM in *E. coli* (33).

Gp28 model: OM-disrupting phage-encoded AMP

Cathelicidin AMPs and gp28 share many structural features, including short length (<60 aa), α-helicity, amphiphilicity, membrane association, and positive charge. These structural features contribute to the membrane-disrupting function that is also shared between the two. In standard AMP assays such as determining the minimum inhibitory concentration (MIC) and minimum bactericidal concentration (MBC), gp28 performed equivalently to LL-37. Based on these data, our model is that gp*28* is an AMP produced by phage for OM disruption during lysis (10).

CHAPTER II

MATERIALS AND METHODS

Bacterial strains, bacteriophages, plasmids, primers and growth conditions

The bacterial strains, bacteriophages, and plasmids used in this study are listed in Table 1. Primers used in this study are listed in Table 2. Bacterial strains were grown in LB media with addition of ampicillin (100 µg/ml), kanamycin (40 µg/ml), chloramphenicol (10 µg/ml), and 10 mM $MgCl_2$ (to stabilize the OM) when appropriate.

Overnight cultures were diluted 1:200 in LB with the above antibiotics. Growth was monitored by following the OD at 550 nm (A_{550}). Bacterial strains were grown with aeration by shaking in a waterbath shaker at 250 rpm at 37ºC until ~0.25 A_{550}. For expression of gp28 in the two-plasmid induction system with pQ and pRE, cultures were induced with a final concentration of 1 mM isopropyl-β-D-thiogalactopyranoside (IPTG) unless otherwise indicated. For induction of λ lysogens with the temperature-sensitive cI_{857} allele, cultures were grown at 30ºC until ~0.25 A_{550} when cultures were thermally induced at 42ºC for 15 min with further growth at 37ºC. For induction of plasmids under araBAD transcriptional control, 0.2-0.4% arabinose was added when indicated.

Table 1. Bacterial strains, bacteriophages, and plasmids

Bacteriophages	Genotype	Source
PhiKT		(20,34)
λ900S_{am}	λ stf::cam cI_{857} $S_{am7}RRzRz1$ bor::kan; Cam^R, Kan^R	(11)
λ900R_{am}	λ stf::cam cI_{857} $SR_{am}RzRz1$; R_{Q26am} and R_{W73am}; Cam^R	(35)

Table 1. Continued

Strains	**Genotype**	**Source**
λ900*Rz$_{am}$Rz1$_{am}$*	λ cI$_{857}$ *SRRz$_{am}$Rz1$_{am}$* bor::kan; Kan^{R}	(36)
RY16390	MG1655 lacI^{q} ΔlacY ΔtonA	Lab stock
MG1655 λ900	RY16390 lysogenized with λ900	(10)
MG1655 λ900*S$_{am}$*	RY16390 lysogenized with λ900*S$_{am}$*	Lab stock
MG1655 λ900*R$_{am}$*	RY16390 lysogenized with λ900*R$_{am}$*	Lab stock
MG1655 λ900*Rz$_{am}$Rz1$_{am}$*	RY16390 lysogenized with λ900*Rz$_{am}$Rz1$_{am}$*	(10)
MG1655 λ900*Rz$_{am}$Rz1$_{a}$*m	RY16390 lysogenized with λ900*S$_{am}$RRz$_{am}$Rz1$_{am}$*	Lab stock
MG1655 λ900*S$_{am}$RRz$_{am}$Rz1$_{a}$*m		(20,34)
4s		
Plasmids	**Genotype**	**Source**
pRE	Medium copy plasmid containing Q-dependent λ late promoter pR'; Amp^{R}	Lab stock
pQ	λ Q transcription factor cloned under P$_{lac/ara-1}$ promoter in a low copy number plasmid pZS-24*; Kan^{R}	Lab stock
pRE gp28	pRE containing PhiKT gene 28	(10)
pRE gp28-his	pRE containing PhiKT gene 28 fused at the C-terminus to the hexahistidine tag GGHHHHHHGG	(10)
pRE gp28-his S2C	pRE gp28-his with the mutation S2C	(10)
pRE gp28-his K16C	pRE gp28-his with the mutation K16C	(10)
pRE gp28-his H18L	pRE gp28-his with the mutation H18L	(10)
pRE gp28-his H18Y	pRE gp28-his with the mutation H18Y	(10)
pRE gp28-his I22N	pRE gp28-his with the mutation I22N	(10)

Table 1. Continued

Plasmids	Description	Source
pRE gp28-his I22T	pRE gp28-his with the mutation I22T	(10)
pRE gp28-his A27D	pRE gp28-his with the mutation A27D	(10)
pRE gp28-his K34M	pRE gp28-his with the mutation K34M	(10)
pRE gp28-his S42C	pRE gp28-his with the mutation S42C	(10)
pRE gp28-his L46P	pRE gp28-his with the mutation L46P	(10)
pRE gp28-his K51X	pRE gp28-his with the mutation K51X	(10)
pRE gp28 K16C	pRE gp28-his K16C with a stop codon introduced before the His-tag	(10)
pRE gp28 L46P	pRE gp28-his L46P with a stop codon introduced before the His-tag	(10)
pRE gp28-TC	pRE gp28 fused at the C-terminus to the tetracysteine (TC) tag GGCCPGCCGG	This study
pRE TC-gp28	pRE gp28 fused at the N-terminus to the tetracysteine (TC) tag MGCCPGCCGG	This study
pRE sec-gp28	pRE gp28 with a PhoA signal sequence	This study
pRE sec-gp28-his	pRE gp28-his with a PhoA signal sequence	This Study
pSec-sfGFP	ss-PhoA-sfGFP; Cam^R	This study
pSecR	ss-PhoA-R; Cam^R	This study
pR-cmyc	R-cmyc; R with c-myc epitope; Cam^R	This study
pR-lacZ	R-lacZ; R-ß-galactosidase fusion; Cam^R	This study

Table 2. Primers and DNA constructs

Primers	Sequence (5' – 3')
pRE for	TTTTACACATGACCTTCGTGA
pRE rev	AGGCAAATTCTGTTTTATCAGA

Table 2. Continued

Primers	**Sequence (5' – 3')**
For gp28 muta	AGCAAATCCCCTTAGGTACCGGCTGAATGCTCCGTATACACAACTGGAGAC
Rev gp28 muta	AAAACAGAAGCTTGGCTGCAGGTCGACGGATCCGTGGTC
pRE gib for	TTGTGACCACGGATCCGTCGACCTGCAGC
pRE gib rev	CGGAGCATTCAGCCGGTACCTAAGGGGATTTGCTCTATTTAATTAGGAATA AGG
Gene Fragments	**Sequence (5' – 3')**
gp28-TC	ATCCCCTTAGGTACCGGCTGAATGCTCCGTATACACAACTGGAGACTTTAA TGAGTAAATTCAAGAAATATCTGGGTGCCGCATGGGATTTCACCAAGGAAC ATGGTGTGACTATCCTGCGTGGTGTGGCTGTCCTCCTTGTAGGTCGTAAGG TTGGTCGCGTTGCCAACCAGTCCGCCGATGTACTTGATACGGTCATCAAAG GGACTAAGAAGAATGGGGGGTGTTGTCCCGGGTGTTGTGGGGGGTAAAGGA TAGCCATGTTCGAAGGCACCGGGAACTACGGTTCCCTTGTGACCACGGATC CGTCGACCTGCAGCCAAGCTTCT
TC-gp28	ATCCCCTTAGGTACCGGCTGAATGCTCCGTATACACAACTGGAGACTTTAA TGGGGTGTTGTCCCGGGTGTTGTGGGGGAATGAGTAAATTCAAGAAATATC TGGGTGCCGCATGGGATTTCACCAAGGAACATGGTGTGACTATCCTGCGTG GTGTGGCTGTCCTCCTTGTAGGTCGTAAGGTTGGTCGCGTTGCCAACCAGT CCGCCGATGTACTTGATACGGTCATCAAAGGGACTAAGAAGAATTAAAGGA TAGCCATGTTCGAAGGCACCGGGAACTACGGTTCCCTTGTGACCACGGATC CGTCGACCTGCAGCCAAGCTTCT

Nonfunctional spanin complementation assay

Assay performed as described previously (36). In summary, MG1655 (RY16390) was lysogenized with λ900*SRRz*$_{am}$*Rz1*$_{am}$. These cells were made competent using the previously described Chung method (37). Plasmids encoding gp28 and mutants were transformed into MG1655 λ900*SRRz*$_{am}$*Rz1*$_{am}$ cells. These λ lysogens were cultured as described above, and OD550 measurements were taken to generate a lysis curve.

Toxicity test

MG1655 (RY16390) carrying the pQ plasmid was transformed with plasmids encoding gp*28* and mutants. These cells were cultured as described above and OD550 measurements were taken to generate a growth curve. Drops in the OD550 indicate toxicity to a growing culture.

Fluorescence microscopy

sec-sfGFP and Sytox Orange

0.4% arabinose was added to the subculture to induce expression of sec-sfGFP. Cultures were grown for ~1.5 hr at 37ºC to reach 0.3-0.4 A_{550} to allow sufficient transport of sfGFP into the periplasm. For time-lapsed population data imaged at 40x, samples were collected at 25, 50, and 75 min after IPTG induction of gp*28*. For extended time lapse data, additional samples were collected at 100 and 125 min after IPTG induction. All samples were prepared and monitored as follows: a 2.5 µl aliquot of sample was placed on a glass slide and covered with a coverslip. Cells were imaged immediately using a plan-neofluar 40x/0.75 Ph2 objective installed on a Zeiss Axio Observer 7 inverted microscope for population data. Samples for single-cell time lapse analysis were collected 30 min after IPTG induction and imaged using an alpha plan-apochromat 100x/1.46 oil (UV) Ph3 M27-oil objective. GFP channel exposure was set to 50 ms for 40x population data and 25 ms for 100x single cell analysis. Sytox channel exposure was set to 40 ms for 40x population data and 20 ms for 100x single cell analysis. Time-lapse videos were captured at 2 fps for approximately 100 min.

ThT and Sytox Orange

Thioflavin-T (ThT) was purchased from Sigma-Aldrich (St. Louis, MO); stocks were made in filter-sterilized water and kept at -20°C prior to use. Sytox Orange was purchased from Thermo Fisher (Waltham, MA). Stocks were made in filter-sterilized water at 100 µM and kept

at -20°C prior to use. Before use, Sytox Orange was diluted 1:100 in sterile Milli-Q water to a concentration of 1 µM.

For population data, 89 µl samples were collected at 25, 50, and 75 min after IPTG induction. ThT and Sytox Orange were added to cells in LB at final concentrations of 10 µM and 0.1 µM, respectively. ThT and Sytox channel exposure were set to 125 ms for 40x population data.

Genetic screening

A template for mutagenesis was created by amplifying the coding sequence of gp*28* using the primers pRE for and pRE rev. Mutagenesis of this template was performed according to the GeneMorph II Random Mutagenesis kit protocol (Agilent Technologies, Santa Clara, CA). The mutagenized gp*28* insert was cloned into an empty pRE vector, transformed into XL1-Blue carrying the pQ plasmid, and plated on LB agar plates supplemented with ampicillin, kanamycin, and IPTG. We simultaneously screened for functional and nonfunctional mutants based on colony opacity. After isolating gp*28* mutants, they were transformed into lysogens carrying the λ900$Rz_{am}Rz1_{am}$ prophage to test for complementation of the lysis defect associated with nonfunctional spanins.

Western blotting

Protein samples were collected as described previously (17). Briefly, a 1 ml aliquot of whole-cell sample was taken at the indicated times and precipitated with ~10% (v/v) cold trichloroacetic acid (TCA). Then, samples were washed twice by ice-cold acetone. TCA pellets were resuspended in a volume of nonreducing Laemmli buffer (2% SDS, 15 mM Tris HCl, pH 8.5, bromophenol blue dye) normalized to the OD550 units at the time of collection after the acetone evaporated completely. For reducing conditions, 1.4% (v/v) β-mercaptoethanol was

added to the Laemmli buffer when indicated. After 5 min of boiling, 30 µL of sample (corresponding to 0.3 OD units) were resolved on a Novex 10-20% Tris-Tricine SDS-PAGE gel (Thermo Fischer, Waltham, MA) with a 1X tris tricine running buffer (100 mM tris, 100 mM tricine, 0.01% SDS). Gel transfer onto a polyvinylidene fluoride membrane and immunodetection were done using the iBlot and iBind systems (Thermo Fisher, Waltham, MA) according to the manufacturer's recommended protocol. Loading controls were performed by staining the membrane with the reversible protein dye Ponceau S (0.1% w/v Ponceau S, 1% v/v acetic acid). Membranes were rocked at room temperature in Ponceau S for up to 1 hr and washed twice for 10 min. The stained membrane was imaged using an Amersham Imager 600 RGB (GE, Pittsburgh, PA) using colorimetric epi-illumination. Membranes were blocked in a solution of 4% milk/TBS (25 mM Tris pH 7.5, 150 mM NaCl) for 1 hr at room temperature or overnight at ~4ºC. A mouse anti-His primary antibody (Thermo Fischer, Waltham, MA) for detection of His-tagged gp*28* was diluted 1:2000 in 1x iBind solution, and a goat-anti-mouse-HRP secondary antibody (Thermo Fischer, Waltham, MA) was diluted 1:1000 in 1x iBind solution. For detection of gp*28*, a rabbit anti-gp*28* primary antibody (GenScript, Piscataway, NJ) was diluted 1:2000 in 1x iBind solution. A goat-anti-rabbit-HRP secondary antibody (Thermo Fischer, Waltham, MA) was diluted 1:1000 in 1x iBind solution. Membranes were developed using SuperSignal West Femto Luminol/Enhancer solution and Stable Peroxide according to directions (Thermo Scientific, Waltham, MA) immediately prior to chemiluminescence scanning with an Amersham Imager 600 RGB. Densitometry was performed using ImageStudioLite (LI-COR Biosciences, Version 5.2.5).

CHAPTER III

RESULTS

Genetic characterization of gp*28*

Given that helical motifs are functionally important for AMPs, we hypothesized that we could probe the peptide structure of gp*28* genetically. Using a genetic screen on a randomly mutagenized gp*28*-his (10), we anticipated the isolation of certain classes of mutations that would be validated through our lysis curve λ complementation assay. Indeed, we show that the proline mutation gp*28*-his L46P is not functional when co-expressed with the λ holin and endolysin (Figure 2A). This result supports not only that gp*28* has helical content but also that one helix within gp*28* contains residue 46. The mutant gp*28*-his I22N is nonfunctional (Figure 2D). Residue I22 is part of the hydrophobic face of a predicted α-helix (Figure 1C), so the addition of the polar asparagine residue may diminish the hydrophobic contact with the membrane. Furthermore, high cationic charge is characteristic of cathelicidins, and changes in the charge distribution tend to alter the function of gp*28*. Gp*28*-his H18L and K34M mutants are reductions in positive charge and are not functional for lysis (Figure 2D). Adding negative charge with the mutant A27D is also nonfunctional (Figure 2D). H18L, K34M, and A27D, though nonfunctional, are proteins that still accumulate (Figure 2F). This suggests that the reason these alleles are nonfunctional is potentially due to the reasons mentioned above and not because the protein is proteolytically unstable. The nonsense mutant K51X is surprisingly nonfunctional (Figure 2E). This mutant allele is only six residues short of WT gp*28* but has three less lysines, a relatively large decrease in positive charge. Interestingly, the mutants H18L and I22N are nonfunctional, but the mutants H18Y and I22T are functional (Figure 2D).

Noticeably, there are no cysteine residues in gp*28* (Figure 1A). The periplasm of Gram-negative bacteria is an oxidative environment (38), which can oxidize thiols in cysteines to disulfides. Oxidation of Cys gp*28* mutants could lead to oligomerization (preliminary data) that can cause an early onset of lysis (Figure 2A&C). The gp*28*-his S2C and S42C alleles were created by site-directed mutagenic PCR to test for changes in gp*28* function resulting from the single-atom change between Ser and Cys. Based on the onset timing of lysis and the terminal time of lysis (defined as the time the A_{550} drops below 0.01), S2C behaves like WT gp*28*-his (Figure 2C). The K16C allele causes lysis to begin approximately 20 min early but completes lysis only ~5 min early (Figure 2C). The S42C allele shockingly causes lysis to occur within 15 min and completes lysis within 20 min.

In addition to lysis curves, we performed "toxicity tests" by expressing only the gp*28* mutants with the two-plasmid induction system. Unlike during lysis in which cells are rapidly bursting, expression of gp*28* alone does not result in a sharp drop in OD within 50 min (Figure 2B). This is because expression of gp*28* alone does not cause lysis. Thus, we use this assay to interpret the toxicity of gp*28* mutants. The early lyser gp*28*-his K16C is toxic to the cell after ~40 min as noted by the drop in OD, and the nonfunctional allele L46P is not toxic based on these data (Figure 2B). The most interesting result is the difference in toxicity between gp*28* and gp*28*-his. In lysis experiments, the difference is not as noticeable (Figure 2A), but our data suggests that gp*28*-his is more toxic that the native gp*28* (Figure 2B). Gp*28* appears to lag behind gp*28*-his in activity (Figure 3C & 4E) and does not appear as toxic as gp*28*-his (Figure 2B & 5A).

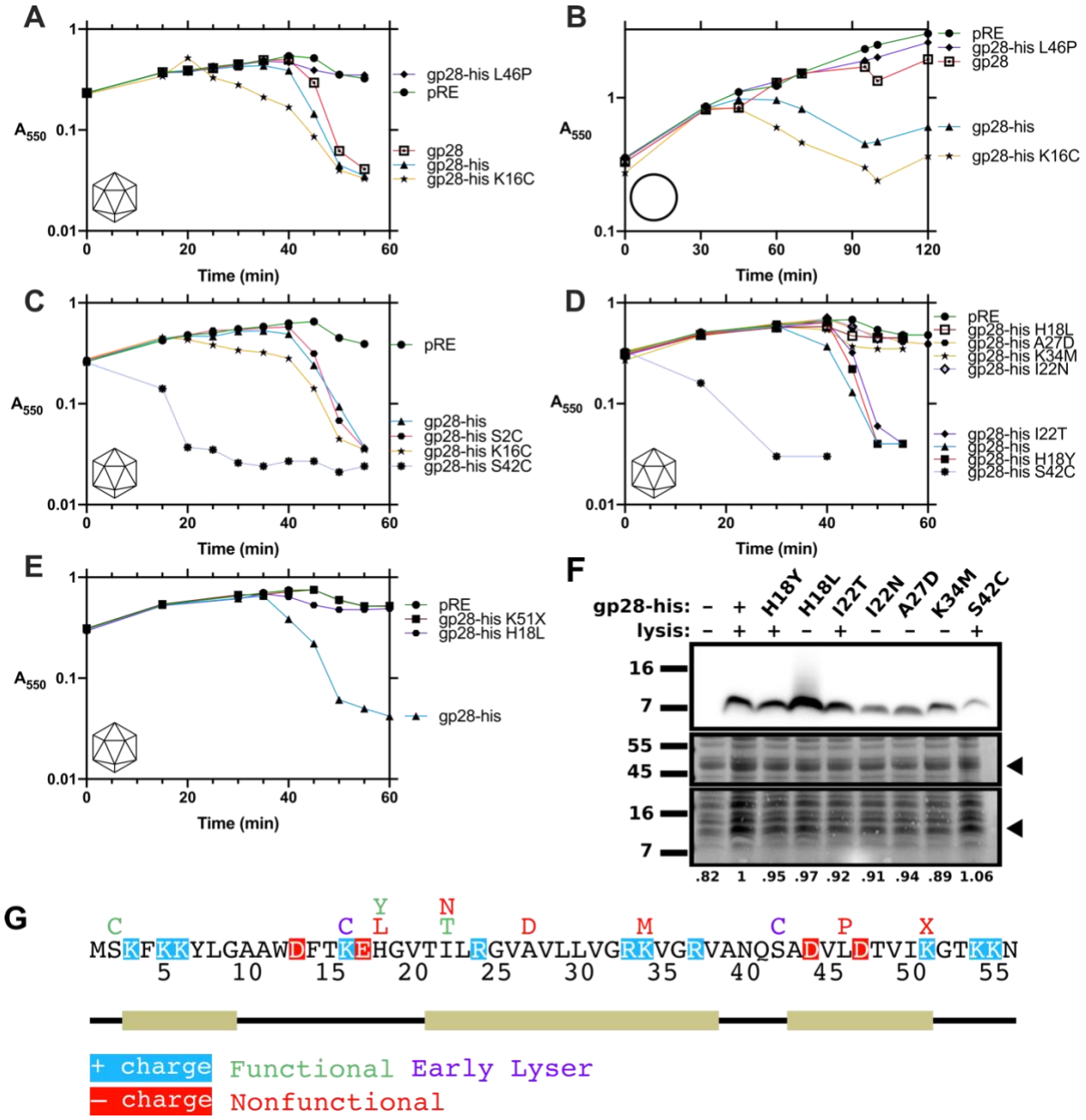

Figure 2. Gp*28* mutants support structural predictions. For all lysis curves, the icosahedron capsid icon in the bottom left means that the bacterial background is a lysogen and is thermally induced. The circle in the bottom left means that the bacterial background is MG1655 (RY16390), and the induction system is the two-plasmid lysis system involving pRE and pQ. Time t=0 is the time of induction. **A, C–E)** Lysis curve of gp*28* mutants in MG1655 *SRRz*$_{am}$*Rz1*$_{am}$ background. **B)** Growth curve of gp*28* mutants in MG1655 (RY16390) background carrying the pQ plasmid. The only lysis proteins expressed are gp*28* mutants. **F)** Western blot of the gp*28* mutants in D). Below: the Ponceau S stained membrane as a sample loading control. The numbers below represent densitometry analysis. Gp*28*-his bands are relative the band between 45 and 55 kDa with gp*28*-his set as a relative intensity of 1. **G)** Summary of mutagenesis presented in this study.

Gp*28* affects both IM and OM permeability

AMPs have been shown to disrupt both membranes in *E. coli* (33), so we aimed to characterize the nature of disruption caused by gp*28*. Theoretically, gp*28* only needs to transiently permeabilize the OM to allow the turgor pressure to complete lysis because of the degradation of the PG. To test how expression of gp*28* affects the membrane permeability, we used a two-fluorophore system with secreted sfGFP and Sytox Orange to monitor the fate of the periplasm. Expressing secreted sfGFP loads the periplasm with a halo of GFP signal, and we can monitor disturbances in this halo to make inferences about membrane permeability when simultaneously using the live-dead stain Sytox Orange (Figure 3A&D). Both the IM and the OM are reported to be impermeable to Sytox Orange (Thermo Fisher), so both must be disrupted for Sytox Orange to stain the nucleoid. While the halo of GFP signal in the empty vector controls does not change, gp*28* alleles that cause disruption of the OM force GFP out of the cell due to the loss of turgor pressure (Figure 3A). Sec-sfGFP is secreted via the sec translocon, which only exports unfolded proteins (39). Unexpectedly, we observe a large increase in cytoplasmic sfGFP signal (Figure 3A). A plausible explanation is that the rates of accumulation and folding of sfGFP are greater than the sec translocon can handle. Eventually, disruption of both membranes is enough to allow Sytox Orange to enter the cell and stain nucleic acids (Figure 3A). These results indicate that gp*28*, like the AMP LL-37 (33), can permeabilize both membranes. This result was not expected for an OM-disrupting lysis protein since the holin exists to open a hole in the IM.

The results of testing the gp*28*-his mutants L46P and K16C in this assay are as expected based on their respective lysis phenotypes. L46P does not disrupt the GFP halo (Figure 3B).

K16C not only disrupts the GFP halo but also can disrupt both the IM and OM to allow Sytox Orange to stain the nucleoid. In addition, the change in the population that does and does not stain Sytox Orange is faster than the gp*28*-his allele (Figure 3B). This result supports the initial observation that K16C causes early lysis.

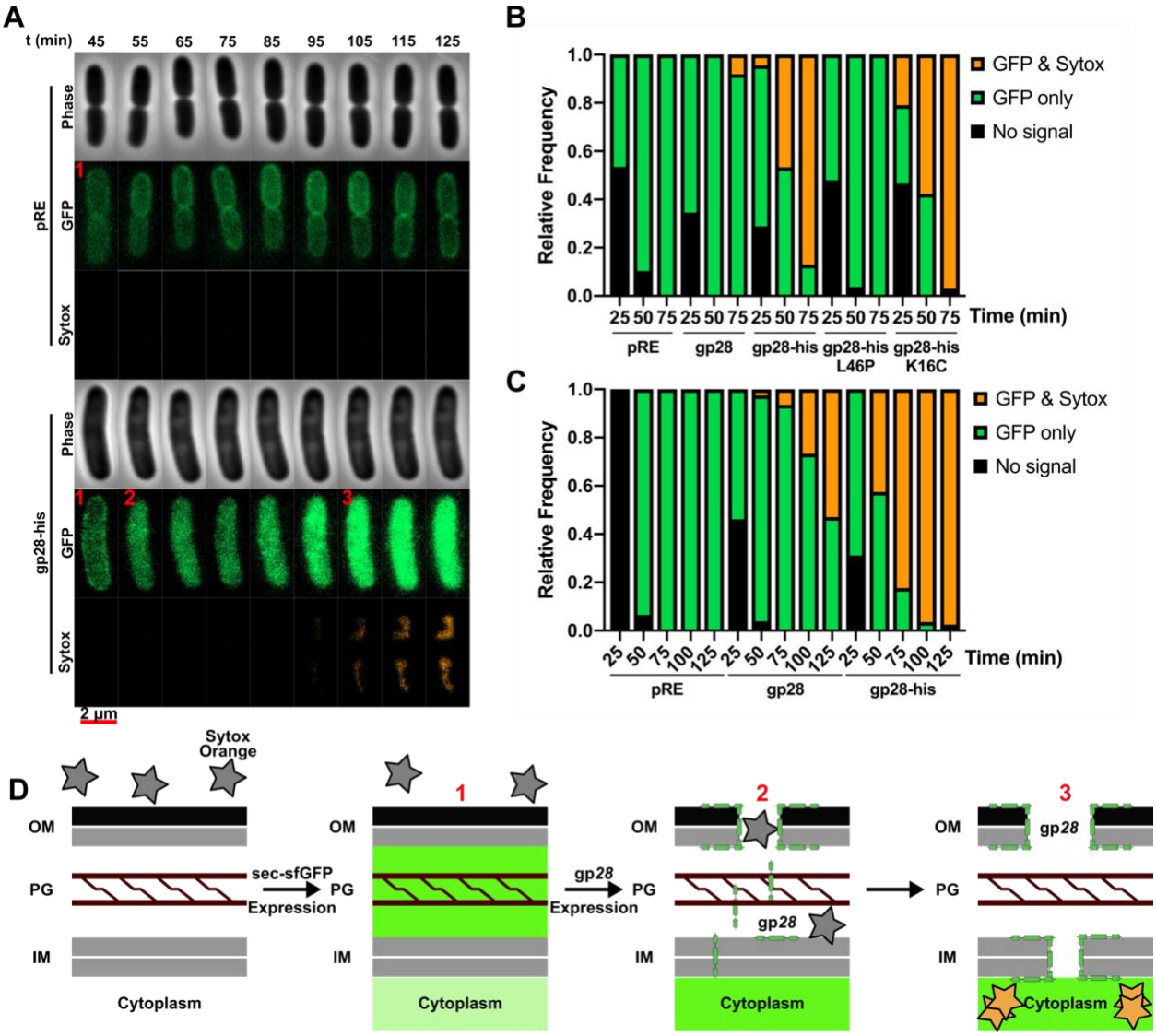

Figure 3. Gp*28* causes GFP leakage out of the periplasm. Time t=0 is the time of induction of gp*28* expression. **A)** 100x time-lapsed micrographs following a representative single cell expressing secreted sfGFP and pRE (top) or pRE gp*28*-his (bottom). Scale bar is 2 µm. The red numbers correspond to the stages of the assay explained in D). **B)** Time course data showing the change in relative frequency of cells with no fluorescent signal, fluorescing with only secreted sfGFP, or with both secreted sfGFP and Sytox Orange. For each timepoint, n = 43–91 cells counted with n_{total} = 934. **C)** Extended time course data similar to B) following only gp*28* and gp*28*-his. For each timepoint, n = 26–124 cells counted with n_{total} = 1023. **D)** Cartoon schematic of the order of events for this assay. Arabinose induction of pSec-sfGFP loads the periplasm with sfGFP, which creates a defined halo of signal in the periplasm. IPTG induction of pRE gp*28* and functional mutants disrupts membranes, which results in the loss of the peripheral GFP signal. Then Sytox enters the cell through permeabilized membranes, staining the DNA and fluorescing.

We then wondered in what order gp*28* disrupts the two membranes of Gram-negative bacteria, given that the role of gp*28* during PhiKT infections is to disrupt the OM. We developed a kinetic assay using a two-dye system with fluorescence microscopy to determine the order of permeabilization. In conjunction with Sytox Orange, Thioflavin-T (ThT) was used to report membrane permeability. Both membranes are impermeable to the nucleoid stain Sytox Orange. ThT has previously been used as a stain for amyloid fibrils (40) and a reporter of RNA metabolism (41). We used ThT as a reporter of IM permeability (Cahill J and Young R, unpublished data). We demonstrated that only the OM but not the IM is normally permeable to ThT (Figure 4D). To validate this two-dye system, we used lysogens carrying λ prophages with a single nonsense mutation in one of the lysis genes. Only lysogens carrying functional holin genes stain with ThT because the holin opens micron-scale holes in the IM (Figure 4B&C). As expected, when the lysogen carries a nonsense mutation in the holin gene and is thermally induced, no ThT staining is observed (Figure 4B&C). Sytox Orange never stains these lysogens because disruption of the OM by a λ lysogen does not happen unless all four λ lysis proteins are functional (Figure 4B&C). When gp*28* and functional mutants are expressed, ThT signal is observed followed by Sytox Orange signal approximately 25 min later (Figure 4D&E). These data suggest that gp*28* can disrupt the IM before the OM.

The mutants K16C and L46P were tested in this assay in both the native gp*28* background and as his-tagged proteins. The K16C mutant appears to disrupt both membranes faster than the parental protein independent of the his-tag (Figure 4E). However, the his-tagged K16C mutant shows a greater frequency of Sytox and ThT staining than the K16C mutant without the his-tag (Figure 4E). This suggests that the gp*28*-his K16C has a greater capacity for membrane disruption than gp*28* K16C. The L46P mutants surprisingly cause the cells to stain

with ThT (Figure 4E) despite being nonfunctional for lysis (Figure 2A). These data suggest that L46P mutants may be associated with the membrane and cause transient permeabilization that is not sufficient for lysis.

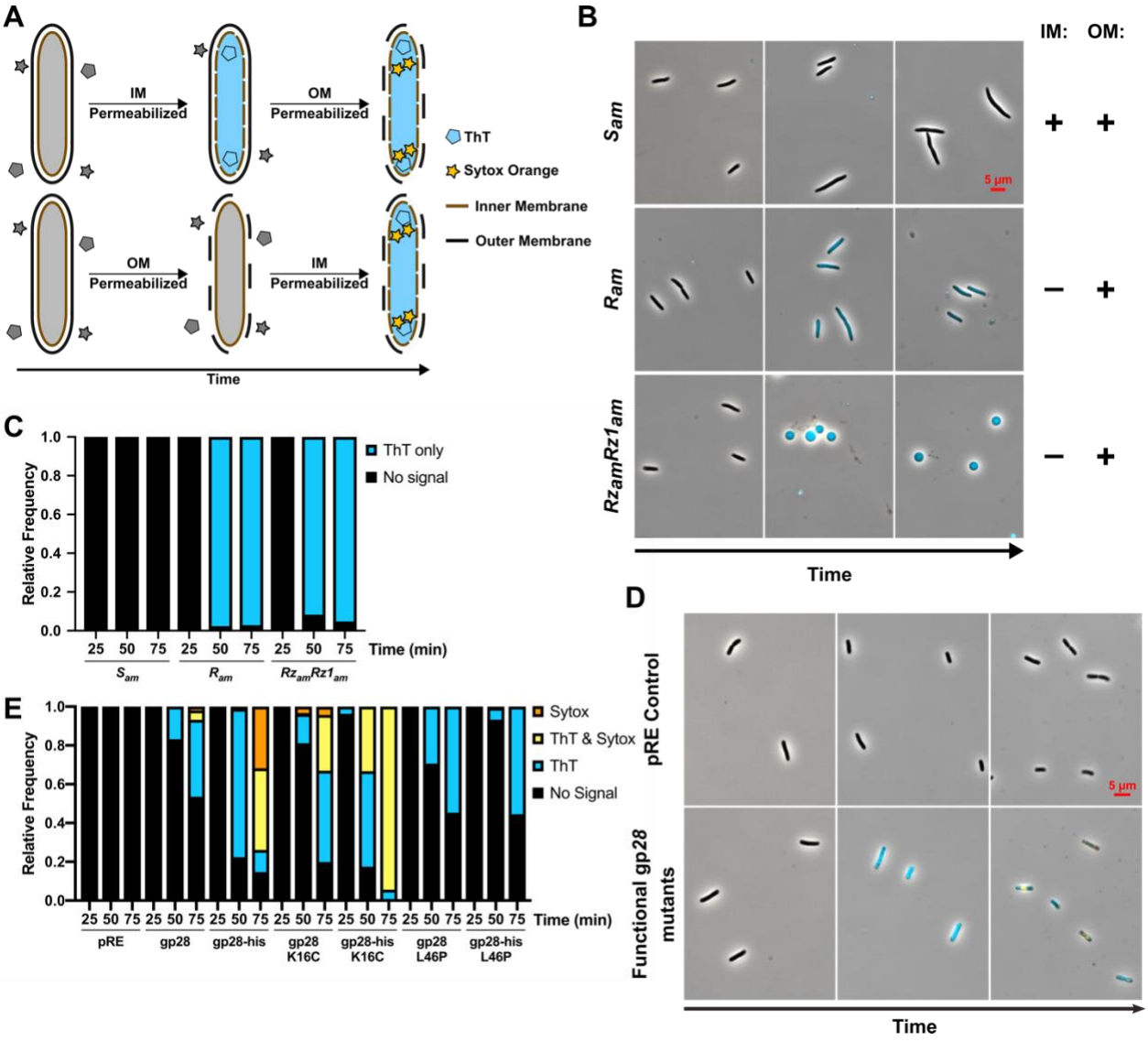

Figure 4. Gp*28* permeabilizes the IM before the OM. A) Cartoon schematic of the ThT/Sytox kinetic membrane permeabilization assay showing the changes in cell fluorescence over time based on the order of membrane disruption. Note: ThT stains nonspecifically, and the fluorescence signal is across the entire cytoplasm. The blue fluorescing ThT pentagons are shown in the cytoplasm for clarity. **B)** Representative 40x micrographs showing a time course of λ900 lysogens used as controls for this assay. Scale bar is 5 µm. Right: + means the membrane is intact and assumed to be undamaged, while – means that the membrane has been disrupted. **C)** Quantification of the time course data with λ lysogens as controls for this assay. For each timepoint, n = 89–139 cells counted with n_{total} = 841. **D)** Representative 40x micrographs showing results that match predictions from A) showing the staining pattern of cells expressing gp*28* (and mutants) compare to an empty vector control. Scale bar is 5 µm. **E)** Time course data showing the change in relative frequency of cells staining with ThT and Sytox Orange. For each timepoint, n = 80–575 cells counted with n_{total} = 5076.

Spanins can disrupt both the IM and OM, but this activity is coupled together since spanins fuse these layers. Gp*28* membrane disruption activity appears to be general and not exclusive to the OM. We aimed to characterize the permeability of the IM upon gp*28* expression using endolysin fusions to report if any holes are made in the IM and what the sizes of these holes are. The λ endolysin is an 18 kDa cytoplasmic protein that cannot cross an intact IM, which necessitates holins. Interestingly, gp*28*-his is able to create holes in the IM large enough to release endolysin, while gp*28* cannot. (Figure 5A&D). As expected, the nonfunctional mutant L46P does not create a hole large enough to release endolysin (Figure 5A). This result further supports that the L46P mutants only transiently permeabilize the IM. Gp*28*-his K16C is capable of disrupting the IM to the extent of endolysin release. To increase the precision of sizing the holes created in the IM, we constructed genes encoding a 19 kDa endolysin fused to a c-myc epitope and a 130 kDa endolysin fused to β-galactosidase (Figure 5). Gp*28*-his and the K16C mutant are capable of releasing the massive R-lacZ endolysin (Figure 5C). In addition, we constructed genes encoding gp*28* and gp*28*-his with the PhoA signal sequence for secretion to test in this experiment. Unsurprisingly, sec-gp*28* was unable to release the R-cmyc endolysin and was assumed to be unable to release the R-lacZ endolysin (Figure 5B). Sec-gp*28*-his, however, demonstrated greater activity than the early lyser mutant K16C (Figure 5B&C). Furthermore, gp*28* mutants (gp*28*-his and gp*28*-his K16C) complement a holin defect to complete lysis in the presence of endolysin and spanins (Figure 5D). This indicates gp*28*-his may disrupt the IM as a consequence of transport to the OM. Overall, these results suggest that gp*28* mutants have potent membrane disruption capacity that parallels holin activity.

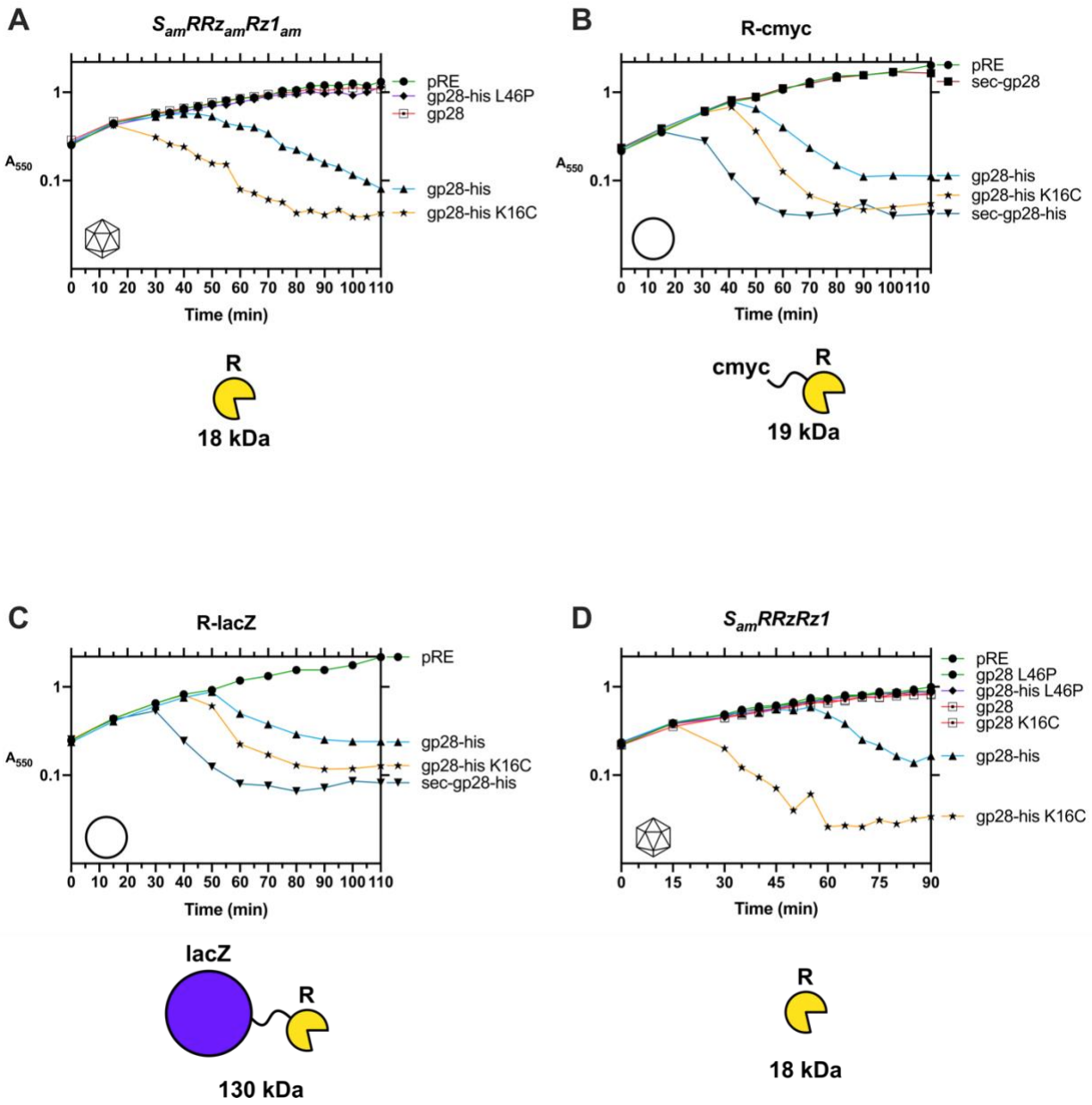

Figure 5. Gp*28* mutants create holes in the IM large enough to release endolysin. A) Lysis curve of gp*28* mutants in the lysogen background MG1655 $S_{am}RRz_{am}Rz1_{am}$. Below: cartoon of a λ endolysin (R) with the molecular weight. **B)** Lysis curve of gp*28* mutants in MG1655 (RY16390) carrying a pZA32 plasmid encoding *R-cmyc*. Below: cartoon of a λ endolysin with the cmyc tag and the total molecular weight of this fusion. **C)** Lysis curve of gp*28* mutants in RY16390 carrying a pZA32 plasmid encoding *R-lacZ*. Below: cartoon of a λ endolysin fused with β-galactosidase (product of *lacZ*) and the total molecular weight of this construct. **D)** Lysis curve of gp*28* mutants in the lysogen background MG1655 $S_{am}RRzRz1$.

CHAPTER IV

DISCUSSION AND CONCLUSION

Genetic analysis of gp*28*

In this study, we presented eleven mutants of gp*28* and gp*28*-his. Disruptions of α-helices (L46P) and changes to the number and distribution of charges (H18L, A27D, K34M, and K51X) result in loss of function, as would be expected of AMPs (see section: Genetic analysis supports model that gp*28* is a phage-encoded AMP). Additionally, we isolated mutants that can cause an earlier onset of lysis (K16C and S42C). Lysis is temporally well-regulated (2), so the drastic change in the onset of lysis may have evolutionary consequences (see section: Gp*28* mutants subvert the holin-controlled onset of lysis). We have not approached saturation in the number of mutants of gp*28*, so we will continue genetic screening for gp*28* mutants. One goal with these mutants would be to localize them within the host cell to test for the interactions contributing to membrane association (see section: Localization of gp*28*).

Genetic analysis supports model that gp*28* is a phage-encoded AMP

Cathelicidin antimicrobial peptides are helical, amphipathic, and cationic and function to disrupt membranes. We have previously shown that gp*28* disrupts the OM of *E. coli* during phage lysis, is cationic, and is predicted to be helical and amphipathic (10). Mutagenesis of gp*28* reveals that residues necessary for α-helical structure are required for function. Prolines prevent the formation of α-helices, so the nonfunctional mutant L46P fails to complement the lysis defect caused by nonfunctional spanins. Mutants that change the charge distribution tend to alter the function of gp*28* as well. Furthermore, AMPs can disrupt both membranes of Gram-negative cells, and we demonstrated that gp*28* has the same function.

Gp*28* mutants subvert the holin-controlled onset of lysis

Given the order of events during lysis, it would be expected that holins control the timing of lysis. When the holin opens a hole in the IM, endolysin degrades the PG. This allows lateral diffusion and oligomerization of spanin complexes to complete λ lysis. Thus, the events of lysis are dependent on the holin disrupting the IM. In fact, holins control the timing of lysis on an allelic basis (42-44). The timing of lysis is subject to selective pressures such as culture density (45). Before lysis occurs, there is a morphogenesis period where progeny virions are produced, and the length of this period determines the number of progeny. In environments with a high cell density, shorter morphogenesis periods are favorable because the phage titer can increase exponentially by further infections (45). Likewise, low cell density cultures favor longer morphogenesis periods, so exponential growth is primarily due to phage production with the cell (45). Because holins have been shown to control the timing of lysis, it is reasonable to conclude that holin genes are the targets of evolutionary pressures to change the timing of lysis. Furthermore, in a genetic analysis of the λ spanins, no mutants expedited lysis (8). Our results indicate that gp*28* can disrupt both the IM and OM despite only being required for OM permeabilization. Additionally, we have identified twelve early lyser mutants (two presented here and the other ten are unpublished data, Cahill, J) that can greatly decrease the timing of lysis, subverting holin control. The data suggest these mutants create holes large enough in the IM to release endolysin (Figure 5A). Another possibility is that these mutants could substantially collapse the proton motive force across the IM, which has been shown to cause the holin to trigger earlier than normal (2). Regardless, gp*28* mutants are capable of changing the timing of lysis, which may not be evolutionarily favorable. Taken together, this would explain why spanins are the most conserved OM disruptors.

Localization of gp*28*

Since gp*28* disrupts the OM, it is logical to conclude that gp*28* must be associated with the OM at some point during lysis. Preliminary data monitoring a GFP-gp*28* construct with fluorescence microscopy suggests that this is the case, but this construct has a different lysis phenotype in terms of timing (Cahill, J, unpublished data). Our strategy was to transition to a small-molecule fluorophore system using a tetracysteine (TC) tag and the dye fluorescein arsenical hairpin binding bis-ethanedithiol adduct (FlAsH-EDT_2) (46). This system has been typically used in eukaryotic systems, but its use has been previously reported in *E. coli* (47-49). We expect that the lysis phenotype of a gp*28*-TC construct will be similar to WT since the size of the TC tag is significantly smaller than GFP (1 kDa and 27 kDa, respectively). Furthermore, we have been successful in staining a TC-tagged protein in the periplasm (Cahill, J, unpublished data) despite the potential for oxidation of the cysteines to disulfides, which prevent FlAsH-EDT_2 binding (46). Thus, we could potentially track gp*28* translocation from the IM to the OM using super-resolution microscopy. Additionally, we aim to test the localization of gp*28* mutants to discern the determinants of membrane association.

REFERENCES

1. Jechlinger, W., Szostak, M. P., Witte, A., and Lubitz, W. (1999) Altered temperature induction sensitivity of the lambda pR/cI857 system for controlled gene E expression in *Escherichia coli*. *FEMS Microbiology Letters* **173**, 347-352

2. Young, R. (1992) Bacteriophage lysis: mechanism and regulation. *Microbiol Rev* **56**, 430-481

3. Berry, J., Summer, E. J., Struck, D. K., and Young, R. (2008) The final step in the phage infection cycle: the Rz and Rz1 lysis proteins link the inner and outer membranes. *Mol Microbiol* **70**, 341-351

4. White, R., Chiba, S., Pang, T., Dewey, J. S., Savva, C. G., Holzenburg, A., Pogliano, K., and Young, R. (2011) Holin triggering in real time. *Proc Natl Acad Sci U S A* **108**, 798-803

5. Berry, J., Rajaure, M., Pang, T., and Young, R. (2012) The spanin complex is essential for lambda lysis. *J Bacteriol* **194**, 5667-5674

6. Berry, J., Savva, C., Holzenburg, A., and Young, R. (2010) The lambda spanin components Rz and Rz1 undergo tertiary and quaternary rearrangements upon complex formation. *Protein Sci* **19**, 1967-1977

7. Kongari, R., Snowden, J., Berry, J. D., and Young, R. (2018) Localization and regulation of the T1 unimolecular spanin. *J Virol* **92**, e00380-00318

8. Cahill, J., Rajaure, M., O'Leary, C., Sloan, J., Marrufo, A., Holt, A., Kulkarni, A., Hernandez, O., and Young, R. (2017) Genetic Analysis of the Lambda Spanins Rz and Rz1: Identification of Functional Domains. *G3 (Bethesda)* **7**, 741-753

9. Berry, J. D., Rajaure, M., and Young, R. (2013) Spanin function requires subunit homodimerization through intermolecular disulfide bonds. *Mol Microbiol* **88**, 35-47

10. Holt, A., Cahill, J., Ramsey, J., O'Leary, C., Moreland, R., Martin, C., Galbadage, D. T., Sharan, R., Sule, P., Bettridge, K., Xiao, J., Cirillo, J., and Young, R. (2019) Phage-encoded cationic antimicrobial peptide used for outer membrane disruption in lysis. *bioRxiv*, 515445

11. Rajaure, M., Berry, J., Kongari, R., Cahill, J., and Young, R. (2015) Membrane fusion during phage lysis. *Proc Natl Acad Sci U S A* **112**, 5497-5502

12. Abdulreda, M. H., and Moy, V. T. (2009) Investigation of SNARE-Mediated Membrane Fusion Mechanism Using Atomic Force Microscopy. *Jpn J Appl Phys (2008)* **48**, 8JA03-08JA0310

13. Risselada, H. J., and Grubmuller, H. (2012) How SNARE molecules mediate membrane fusion: recent insights from molecular simulations. *Curr Opin Struct Biol* **22**, 187-196

14. Harrison, S. C. (2015) Viral membrane fusion. *Virology* **479-480**, 498-507

15. White, J. M., Delos, S. E., Brecher, M., and Schornberg, K. (2008) Structures and mechanisms of viral membrane fusion proteins: multiple variations on a common theme. *Crit Rev Biochem Mol Biol* **43**, 189-219

16. Kongari, R., Rajaure, M., Cahill, J., Rasche, E., Mijalis, E., Berry, J., and Young, R. (2018) Phage spanins: diversity, topological dynamics and gene convergence. *BMC Bioinformatics* **19**, 326

17. Cahill, J., Rajaure, M., Holt, A., Moreland, R., O'Leary, C., Kulkarni, A., Sloan, J., and Young, R. (2017) Suppressor Analysis of the Fusogenic Lambda Spanins. *J Virol* **91**, e00413-00417

18. Fernandes, S., and São-José, C. (2018) Enzymes and Mechanisms Employed by Tailed Bacteriophages to Breach the Bacterial Cell Barriers. *Viruses* **10**, 396

19. Hernandez-Morales, A. C., Lessor, L. L., Wood, T. L., Migl, D., Mijalis, E. M., Russell, W. K., Young, R. F., and Gill, J. J. (2018) Genomic and Biochemical Characterization of Acinetobacter Podophage Petty Reveals a Novel Lysis Mechanism and Tail-Associated Depolymerase Activity. *J Virol* **92**, e01064-01017

20. Knirel, Y. A., Prokhorov, N. S., Shashkov, A. S., Ovchinnikova, O. G., Zdorovenko, E. L., Liu, B., Kostryukova, E. S., Larin, A. K., Golomidova, A. K., and Letarov, A. V. (2015) Variations in O-antigen biosynthesis and O-acetylation associated with altered phage sensitivity in Escherichia coli 4s. *J Bacteriol* **197**, 905-912

21. Drozdetskiy, A., Cole, C., Procter, J., and Barton, G. J. (2015) JPred4: a protein secondary structure prediction server. **43**, W389-W394

22. Gautier, R., Douguet, D., Antonny, B., and Drin, G. (2008) HELIQUEST: a web server to screen sequences with specific α-helical properties. *Bioinformatics* **24**, 2101-2102

23. Eisenberg, D., Weiss, R. M., and Terwilliger, T. C. (1982) The helical hydrophobic moment: a measure of the amphiphilicity of a helix. *Nature* **299**, 371-374

24. Zhang, L.-J., and Gallo, R. L. (2016) Antimicrobial peptides. *Current Biology* **26**, R14-R19

25. Kosciuczuk, E. M., Lisowski, P., Jarczak, J., Strzalkowska, N., Jozwik, A., Horbanczuk, J., Krzyzewski, J., Zwierzchowski, L., and Bagnicka, E. (2012) Cathelicidins: family of antimicrobial peptides. A review. *Mol Biol Rep* **39**, 10957-10970

26. Ritonja, A., Kopitar, M., Jerala, R., and Turk, V. (1989) Primary structure of a new cysteine proteinase inhibitor from pig leucocytes. **255**, 211-214

27. Sorensen, O. E., Follin, P., Johnsen, A. H., Calafat, J., Tjabringa, G. S., Hiemstra, P. S., and Borregaard, N. (2001) Human cathelicidin, hCAP-18, is processed to the antimicrobial peptide LL-37 by extracellular cleavage with proteinase 3. *Blood* **97**, 3951-3959

28. Cowland, J. B., Johnsen, A. H., and Borregaard, N. (1995) hCAP-18, a cathelin/pro-bactenecin-like protein of human neutrophil specific granules. *FEBS Lett* **368**, 173-176

29. Sorensen, O., Bratt, T., Johnsen, A. H., Madsen, M. T., and Borregaard, N. (1999) The human antibacterial cathelicidin, hCAP-18, is bound to lipoproteins in plasma. *J Biol Chem* **274**, 22445-22451

30. Larrick, J. W., Hirata, M., Balint, R. F., Lee, J., Zhong, J., and Wright, S. C. (1995) Human CAP18: a novel antimicrobial lipopolysaccharide-binding protein. *Infect Immun* **63**, 1291-1297

31. Gennaro, R., and Zanetti, M. (2000) Structural features and biological activities of the cathelicidin-derived antimicrobial peptides. *Biopolymers* **55**, 31-49

32. Ebbensgaard, A., Mordhorst, H., Aarestrup, F. M., and Hansen, E. B. (2018) The Role of Outer Membrane Proteins and Lipopolysaccharides for the Sensitivity of Escherichia coli to Antimicrobial Peptides. *Front Microbiol* **9**, 2153

33. Choi, H., Rangarajan, N., and Weisshaar, J. C. (2016) Lights, Camera, Action! Antimicrobial Peptide Mechanisms Imaged in Space and Time. *Trends Microbiol* **24**, 111-122

34. Golomidova, A., Kulikov, E., Isaeva, A., Manykin, A., and Letarov, A. (2007) The Diversity of Coliphages and Coliforms in Horse Feces Reveals a Complex Pattern of Ecological Interactions. **73**, 5975-5981

35. Park, T., Struck, D. K., Dankenbring, C. A., and Young, R. (2007) The Pinholin of Lambdoid Phage 21: Control of Lysis by Membrane Depolarization. *Journal of Bacteriology* **189**, 9135-9139

36. Zhang, N., and Young, R. (1999) Complementation and characterization of the nested Rz and Rz1 reading frames in the genome of bacteriophage lambda. *Molecular & general genetics : MGG* **262**, 659-667

37. Chung, C. T., and Miller, R. H. (1993) Preparation and Storage of Competent *Escherichia coli* Cells *Methods in Enzymology* **218**, 621-627

38. Miller, S. I., and Salama, N. R. (2018) The gram-negative bacterial periplasm: Size matters. *PLOS Biology* **16**, e2004935

39. Du Plessis, D. J. F., Nouwen, N., and Driessen, A. J. M. (2011) The Sec translocase. **1808**, 851-865

40. Xue, C., Lin, T. Y., Chang, D., and Guo, Z. (2017) Thioflavin T as an amyloid dye: fibril quantification, optimal concentration and effect on aggregation. **4**, 160696

41. Sugimoto, S., Arita-Morioka, K.-I., Mizunoe, Y., Yamanaka, K., and Ogura, T. (2015) Thioflavin T as a fluorescence probe for monitoring RNA metabolism at molecular and cellular levels. **43**, e92-e92

42. Chang, C. Y., Nam, K., and Young, R. (1995) S gene expression and the timing of lysis by bacteriophage lambda. *Journal of bacteriology* **177**, 3283-3294

43. Raab, R., Neal, G., Sohaskey, C., Smith, J., and Young, R. (1988) Dominance in lambda S mutations and evidence for translational control. *Journal of Molecular Biology* **199**, 95-105

44. Johnson-Boaz, R., Chang, C.-Y., and Young, R. (1994) A dominant mutation in the bacteriophage lambda S gene causes premature lysis and an absolute defective plating phenotype. *Molecular Microbiology* **13**, 495-504

45. Cahill, J., and Young, R. (2018) Phage Lysis: Multiple Genes for Multiple Barriers. *Advances in Virus Research* **103**, 33-70

46. Albert, G. B., R., A. S., Jay, J., and Y., T. R. (2000) Fluorescent Labeling of Recombinant Proteins in Living Cells with FlAsH. *Methods in Enzymology* **327**, 565-578

47. Romantsov, T., Helbig, S., Culham, D. E., Gill, C., Stalker, L., and Wood, J. M. (2007) Cardiolipin promotes polar localization of osmosensory transporter ProP inEscherichia coli. *Molecular Microbiology* **64**, 1455-1465

48. Romantsov, T., Battle, A. R., Hendel, J. L., Martinac, B., and Wood, J. M. (2010) Protein Localization in Escherichia coli Cells: Comparison of the Cytoplasmic Membrane Proteins ProP, LacY, ProW, AqpZ, MscS, and MscL. **192**, 912-924

49. Copeland, M. F., Flickinger, S. T., Tuson, H. H., and Weibel, D. B. (2010) Studying the Dynamics of Flagella in Multicellular Communities of Escherichia coli by Using Biarsenical Dyes. **76**, 1241-1250